AIAA JOURNAL
Vol. 32, No. 3, March 1994

Interferometric Investigations of Compressible Dynamic Stall over a Transiently Pitching Airfoil

M. S. Chandrasekhara*
Naval Postgraduate School, Monterey, California 93943
L. W. Carr†
NASA Ames Research Center, Moffett Field, California 94035
and
M. C. Wilder‡
MCAT Institute, San Jose, California 95127

The compressible dynamic stall flowfield over a NACA 0012 airfoil transiently pitching from 0 to 60 deg at a constant rate under compressible flow conditions has been studied using real-time interferometry. A quantitative description of the overall flowfield, including the finer details of dynamic stall vortex formation, growth, and the concomitant changes in the airfoil pressure distribution, has been provided by analyzing the interferograms. For Mach numbers above 0.4, small multiple shocks appear near the leading edge and are present through the initial stages of dynamic stall. Dynamic stall was found to occur coincidentally with the bursting of the separation bubble over the airfoil. Compressibility was found to confine the dynamic stall vortical structure closer to the airfoil surface. The measurements show that the peak suction pressure coefficient drops with increasing freestream Mach number, and also it lags the steady flow values at any given angle of attack. As the dynamic stall vortex is shed, an anti-clockwise vortex is induced near the trailing edge, which actively interacts with the post-stall flow.

Nomenclature

C_p = pressure coefficient
c = airfoil chord
M = free stream Mach number
Re = Reynolds number based on c and U_∞
U_∞ = freestream velocity
x,y = chordwise and vertical distance
α = angle of attack
$\dot{\alpha}$ = pitch rate, in deg/s
α^+ = nondimensional pitch rate, $\dot{\alpha}c/U_\infty$
γ = ratio of specific heats
ϵ = fringe number
ρ = density
ρ_0 = density at reference (atmospheric) conditions

I. Introduction

THE utilization of dynamic stall as a method for increasing the maneuverability and agility of aircraft has received significant attention during the past few years. Several researchers[1-6] have studied the flow over pitching airfoils using flow visualization and unsteady pressure measurements and have provided valuable information on the dynamic stall phenomenon. However, all of these studies were at low speeds. Lorber and Carta[7] have obtained measurements under compressibility conditions that showed that at higher Mach numbers the flow could not develop the suction levels observed under incompressible conditions and noted that this effectively limited the stall delay that could be achieved. The computational studies of Visbal[8] lend some support to this result. Since compressibility effects have been shown[9,10] to change the way that dynamic stall develops, a better understanding of these effects has been of interest in the development of supermaneuverable aircraft and highly agile helicopters. It is well known[9] that the effects of compressibility set in at very low freestream Mach numbers (M = 0.2–0.3) on airfoils operating at high-lift levels due to the development of extremely strong suction peaks near the leading edge, which cause acceleration of the local flow to supersonic speed. The fact that dynamic lift still persists even when compressibility effects appear[10] supports the argument that the benefits of dynamic stall can be exploited in flight systems. However, for these attempts to be successful, a better understanding of the effects of compressibility on the developing unsteady flow is needed.

Most of the events of dynamic stall onset are concentrated near the leading-edge region of an airfoil or wing executing unsteady pitch-up motion. These include occurrence of strong suction pressures, rapid movement of the stagnation point, transition of the boundary layer, possible formation of a separation bubble, production of shocks (which can interact with the boundary layer and cause separation), generation of large amounts of coherent vorticity (which becomes the dynamic stall vortex/vorticity), and initial movement of the dynamic stall vortex over the airfoil. In contrast to dynamic stall onset, the later stages of dynamic stall development require knowledge about the flow away from the surface of the airfoil. Global characteristics of the flow are needed to understand the interactions that occur as the vortex moves down the airfoil. As it moves past the trailing edge, additional events such as generation of a trailing-edge vortex, redistribution of the flowfield over the airfoil, etc., occur that need to be documented if the dynamic flow is to be controlled and utilized.

Experiments focused on these issues are ongoing in the Compressible Dynamic Stall Facility (CDSF) at the Fluid Mechanics Laboratory (FML) of NASA Ames Research Center. The primary goal of the research is to improve the understanding of these complex fluid interactions. It is also aimed at

Presented as Paper 93-0211 at the AIAA 31st Aerospace Sciences Meeting, Reno, NV, Jan. 11–14, 1993; received Feb. 9, 1993; revision received Aug. 11, 1993; accepted for publication Aug. 16, 1993.

*Associate Director and Research Associate Professor, Department of Aeronautics and Astronautics, Navy-NASA Joint Institute of Aeronautics, M.S. 260-1, NASA Ames Research Center, Moffett Field, CA 94035-1000. Associate Fellow AIAA.

†Research Scientist and Group Leader, Unsteady Viscous Flows, Aeroflightdynamics Directorate, U.S. Army ATCOM and Fluid Mechanics Laboratory Branch. Member AIAA.

‡Research Scientist.

obtaining quality experimental data to serve as a benchmark for computational studies. A simple real-time technique known as point diffraction interferometry (PDI), which was developed recently and does not have the limitations of standard interferometry methods, has been used to document the flow over an airfoil transiently pitching at a constant rate. A large number of flow interferograms have been obtained and processed to determine the pressure field to assess the role of unsteadiness in achieving stall delay and sustaining dynamic lift. Some of the results of this effort are reported in the present paper.

II. Description of the Facility, Instrumentation, and Experimental Technique

A. Facility

The CDSF is a unique experimental facility of the Navy-NASA Joint Institute of Aeronautics and is operated as part of the in-draft tunnel complex at the FML (for details see Carr and Chandrasekhara[11]). The airfoil is supported in the CDSF between two 2.54-cm-thick optical quality glass windows by small pins, permitting optical access to the complete flowfield. Thus, details of the flow at the surface near the leading edge, where the dynamic stall vortex forms, as well as the flowfield away from the airfoil can be captured.

The transient pitching motion is produced by a feedback controlled, programmable hydraulic drive system. The airfoil is pitched from 0 to 60 deg at rates of up to 3600 deg/s. To limit or isolate the effects of transients on separation, the change in angle of attack during acceleration and the time of acceleration were limited to less than 6 deg and 4 ms, respectively. The system uses both the airfoil position and velocity information in its feedback loops to properly perform the programmed maneuver. The complete details of the design are presented in Chandrasekhara and Carr.[12] The highest pitch rate used in the experiment (on a 7.62-cm-chord airfoil) corresponds to a 90 deg/s pitch rate of a 3-m-chord airplane wing at any given Mach number; thus, the rates obtainable from the study are applicable to flight conditions. It is worth pointing out that this scaling does not fully simulate the boundary-layer scales such as transition and its role on flow separation.

B. Instrumentation

The airfoil position was read by a digital optical encoder, whose output was input to the digital I/O board of a microVAX II workstation and timed with its internal clock. The data obtained showed that the airfoil angle of attack increased at a linear rate as it passed through the static stall angle. At the highest rate, the motion was completed in 18 ms.

The nondimensional pitch rates used are based on the total time for pitching from 0 to 57 deg. However, the hydraulic control system caused the airfoil to pitch 5–8% faster in the 0–10-deg range and sometimes in the 0–30-deg range. This difference is not believed to significantly affect the global results of the study.

C. Point Diffraction Interferometry Technique

The technique used in the study was point diffraction interferometry, which utilizes the ability of a point discontinuity (a pinhole) located at the image of a point source to diffract a portion of the incident light into a spherical reference wave front. In the present application, the primary optics of an existing schlieren system[13] were used with a pulsed Nd:YAG laser as the light source. The laser light was expanded through a microscope objective to fill the schlieren mirror, transmitted through the test section, and refocused by another schlieren mirror. An exposed photographic plate was placed at the focus of this second mirror (replacing the knife edge), and with no flow in the tunnel, the laser was pulsed with enough energy to burn a hole, or spot, in-situ in the emulsion located at the focal plane of the second mirror. The spot was precisely tailored to the application under investigation, automatically correcting for nonuniformities in the light source or optics. With the flow turned on, the laser was triggered externally at the desired angles of attack, and the real-time interference fringes were recorded on ASA 3000 Polaroid film. Further details about the PDI technique can be found in Refs. 13 and 14.

D. Interferogram Image Processing

Digitized (256 gray levels) interferograms were processed semi-automatically on an IRIS workstation to recover the pressure distributions using a specially developed software package. An airfoil was overlayed on the digitized image using the triangular registration markers seen in the photographs. The intersections of the fringes with the airfoil upper and lower surfaces (or the local boundary-layer edge, when detectable) were interactively picked by the user. The density along any fringe was calculated from the Gladstone-Dale equation,[15] which for the present wind tunnel and laser simplifies to

$$\rho - \rho_0 = 0.009421\epsilon$$

As usual, bright fringes have integer values and dark fringes are numbered as half-integers. Fringes from the freestream to the stagnation point have positive values. The corresponding pressure along a fringe, including that at the boundary-layer edge, was derived using isentropic flow relations as

$$C_p = \frac{[(\rho/\rho_0)^\gamma - 1]}{[(\gamma/2)M^2]}$$

This pressure at the edge of the boundary layer was used as the surface pressure invoking the boundary-layer assumptions. Typical processing time was about 3–5 min per image.

In cases where the fringe density was high or the fringes were fuzzy, the user could go into the "off-body" mode and pick fringes along a line parallel to and away from the airfoil surface where the fringes are farther apart. For this purpose, an option to superimpose two larger airfoils over the image on the screen was provided in the software. The fringe intersections on the larger airfoils were then suitably projected onto the actual airfoil surface. At angles of attack near the dynamic stall angle, the fringes near the leading-edge region were very dense, reflecting the large local density gradients. Further, in this region, optical noise introduced by the shadowgraph effect generally lowered the contrast, making it a location where the off-body mode needed to be invoked.

In the present study the entropy change in the vortical flow was ignored (for lack of a better method). Interferograms with shocks have not been processed because of this limitation.

E. Experimental Conditions

Several hundred interferograms of the dynamic stall flowfield over a 7.62-cm-chord, NACA 0012 airfoil at free-stream Mach numbers ranging from 0.2 to 0.45 were obtained at a resolution of 0.5 deg (or better if needed). The corresponding nondimensional pitch rate was varied from 0.020 to 0.040. The Reynolds number of the flow based on airfoil chord ranged from 3.6×10^5 to 8.1×10^5.

The experiments were conducted in two phases. In the first phase, the full flowfield interferograms were obtained for a range of conditions; phase II focused on the leading-edge flow details only.

III. Results and Discussion

The interferogram images will first be discussed qualitatively as flow visualization images. The quantitative pressure distributions derived from the images will be presented in the second part of the section. Although much of the paper is devoted to the leading-edge flow, when appropriate, the full flowfield is also discussed.

A. Discussion of Interferogram Images

1. Separation Bubble and Dynamic Stall

Figure 1 is a point diffraction interferogram of the flow at $M = 0.3$, $\alpha = 12$ deg, and $\alpha^+ = 0.03$. This image reveals some

important features of the flow. The dark closed fringe on the lower surface slightly aft of the leading edge surrounds the stagnation point. The suction pressure developed by the airfoil causes the local flow to accelerate, resulting in strong density changes, which is seen in the figure as a concentration of fringes near the leading edge on the upper surface. The close spacing of the fringes also means that the flow gradients are high. In fact, 21 dark fringes are present within about 1 mm ($x/c \approx 0.1$) in this image, indicating that the local maximum Mach number is 0.71 and the local pressure coefficient is -3.75 at $x/c = 0.01$. Downstream of this point, a steep adverse pressure gradient region develops (see Sec. III.B.3) and flow separation occurs. The separated shear layer reattaches after it makes a transition into a turbulent layer, forming a classical laminar separation bubble. In the figure, the fringes in the bubble appear as lines emanating from the leading edge that turn abruptly toward the upper surface at $x/c \approx 0.05$ and turn sharply again as the local boundary layer is encountered. Inside the bubble, the fringes run parallel to the surface locally, representing the pressure plateau normally associated with laminar separation bubbles. The accompanying pressure distribution (which will be discussed in Sec. III.B.3) obtained with the fringe analysis software shows the suction peak, the drop in suction due to the adverse pressure following it, and the laminar separation bubble, which is indicated by the plateau in the distribution. In the interferograms to be discussed, the features upstream of the bubble are nearly the same, with the exception that more fringes appear with increase in angle of attack. As dynamic stall occurs, differences evolve will be pointed out.

2. *Leading-Edge Supersonic Flow*

Chandrasekhara et al.[16] found that the airfoil leading-edge flow can become supersonic, leading to formation of multiple shocks. Figure 2 provides quantitative documentation of this. Depending on the angle of attack, a shock or multiple shocks form in the flow. Figure 2 shows a PDI image for $M = 0.45$ at $\alpha = 12.6$ deg and $\alpha^+ = 0.0313$. Fringe counting shows that the local Mach number ahead of the first shock—at a height of $y/c \approx 0.04$—is greater than 1.0 and is about 1.2 at its foot. Although the flow is only weakly supersonic, the shock causes the leading-edge laminar boundary layer to separate.[16] This separated free shear layer develops waviness, which causes the flow downstream of the shock to go through a series of accelerations and decelerations. As the flow negotiates the crests and valleys of this wavy shear layer, expansion waves and compression waves develop, causing the series of shocks. The last shock in the series appears to be the strongest, and the flow becomes subsonic downstream. The occurrence of multiple shocks is repeatable, and the shocks were found to be present over an angle-of-attack range of about 1 deg.

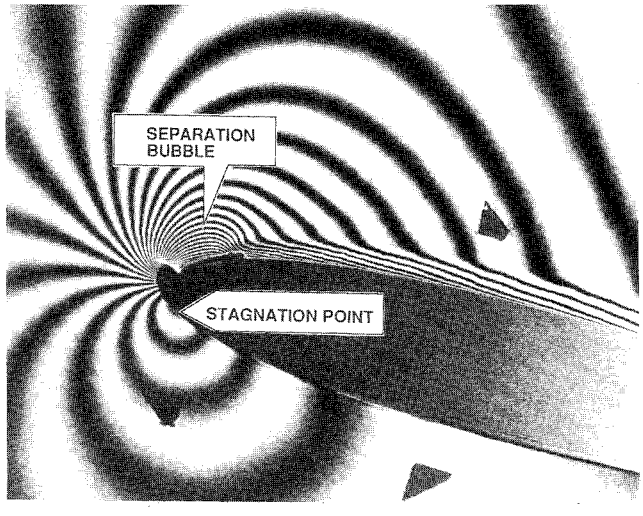

Fig. 1 Point diffraction interferogram; $M = 0.3$, $\alpha = 12$ deg, and $\alpha^+ = 0.03$.

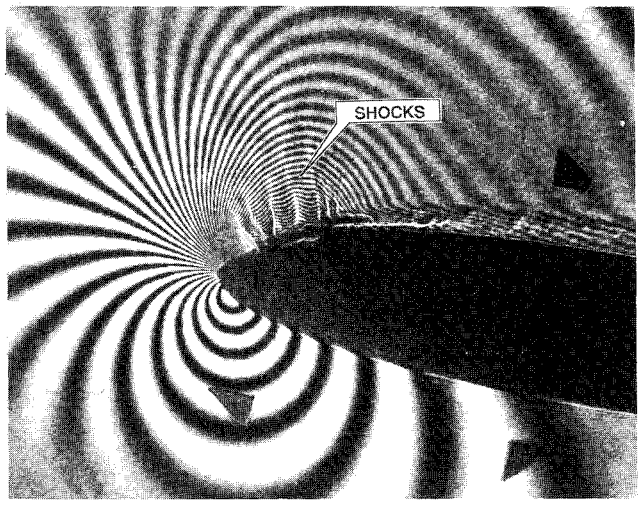

Fig. 2 Multiple shocks over a rapidly pitching airfoil; $M = 0.45$, $\alpha = 12.6$ deg, and, $\alpha^+ = 0.0313$.

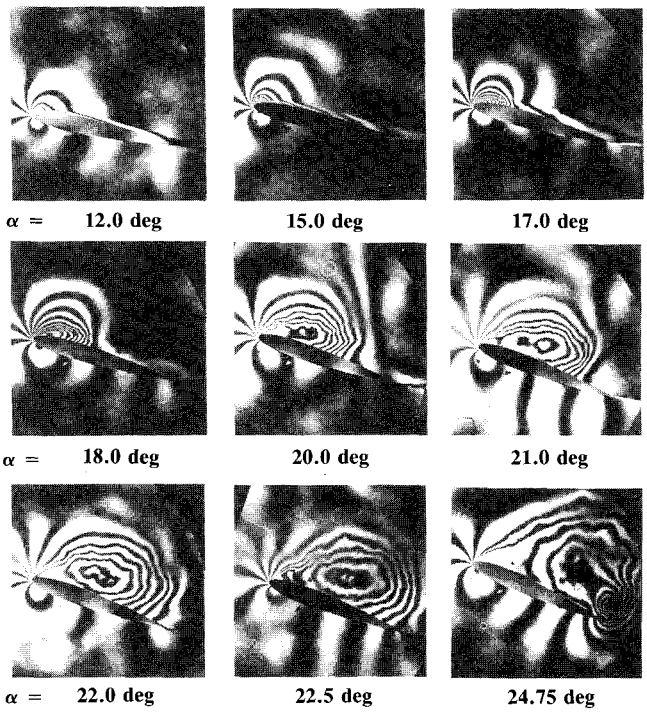

Fig. 3 Dynamic stall flow development over a transiently pitching airfoil; $M = 0.2$ and $\alpha^+ = 0.03$.

3. *Flow Description at $M = 0.2$ and $\alpha^+ = 0.03$*

Figure 3 presents a montage of interferograms for $M = 0.2$ at a nondimensional pitch rate of 0.03 for $12 \leq \alpha \leq 24.75$ deg. A separation bubble is present for $\alpha = 12$ deg; analysis of the interferograms showed that the bubble first appeared at $\alpha = 7$ deg (as opposed to about 6 deg in steady flow at $M = 0.2$). At $\alpha = 15$ deg, the upper surface fringe near the trailing edge indicates a mild local flow separation as this fringe first moves into the wake and turns sharply back toward the trailing edge. Also, the leading-edge bubble starts to open up, and the first imprint of the dynamic stall vortex becomes distinct at $\alpha = 17$ deg. As it grows, the enveloping shear layer moves downstream, and the airfoil boundary layer thickens. The growth of the vortex continues while it convects over the airfoil during the continuous ramping motion. For example, at $\alpha = 18$ deg, the center of the vortex is at $x/c = 0.1$, but the downstream

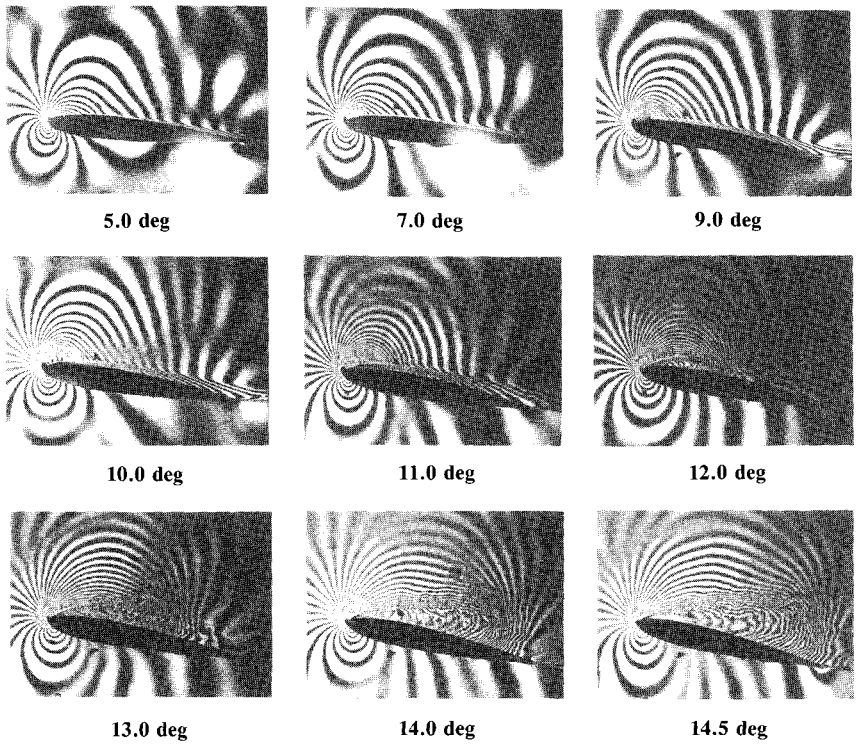

Fig. 4 Dynamic stall flow development over a transiently pitching airfoil; $M = 0.45$ and $\alpha^+ = 0.02$.

edge of the surrounding shear layer is at $x/c = 0.3$. The number of fringes is seen to increase until $\alpha = 18$ deg, demonstrating that the low-pressure region continues to grow. By $\alpha = 20$ deg, the leading-edge flow has separated, and the fluid aft of the shear layer enclosing the vortex has been convected past the trailing edge, and thus no fringes can be seen in this region. Once the vortex grows and begins to convect, the innermost fringes become circular (for example at $\alpha = 21$ and 22 deg), whereas the outer fringes still end on the surface. The number of fringes inside the vortex is now larger than that at the leading edge. This implies that the pressure in the vortex core is lower than the peak suction over the airfoil. Surface pressure measurements, however, cannot reveal this. The vortex is eventually shed by $\alpha = 24.75$ deg, and the flow reaches the deep stall state. A counterclockwise trailing-edge vortex also forms at this angle of attack. For this test condition, the vortex remains over the surface for a large angle-of-attack range of 12 deg. Similar studies on an oscillating airfoil ($\alpha = 10° + 10° \sin \omega t$) at $M = 0.2$ showed that deep stall occurred at $\alpha = 18.1$ deg. The presence of the dynamic stall vortex until $\alpha = 24.75$ deg elicits the fact that motion history plays a key role in the dynamic stall process. In this case, the transiently pitching airfoil is found to be better than oscillating airfoils in sustaining the dynamic lift generated.

4. Flow Sequence at $M = 0.45$ and $\alpha^+ = 0.02$

Figure 4 shows a similar set of interferograms for $M = 0.45$ at a nondimensional pitch rate of 0.02. At this Mach number, compressibility effects dominate.[16] The large number of fringes seen at low angles of attack is due to the larger density changes in the flow at this higher Mach number. The innermost closed fringe intersecting the lower surface near the leading edge encloses the stagnation point. There are 58 fringes (corresponding to a local Mach number of ≈ 1.2) around the leading edge in the first 1.5% of the airfoil chord at $\alpha = 9$ deg. A separation bubble forms in this case also and is seen clearly at $\alpha = 7$ deg. In steady flow at this Mach number, the bubble was first seen for $\alpha = 5$ deg. Thus, a delay is observed in its first appearance in the unsteady case. At $\alpha = 9$ deg, the first signs of the dynamic stall vortex/vortical structure are seen as a thin shear layer between the bubble and the airfoil upper surface near the leading-edge region (see also Fig. 5). Multiple shocks similar to those discussed in Fig. 2 form in this case also. The shocks remain on the surface until $\alpha = 11$ deg, even after the dynamic stall process is well under way. It is not yet clear whether the first shock-induced boundary-layer separation caused the dynamic stall vortex to form.

The vortex grows with increasing angle of attack as the shear layer enveloping it reattaches further down the airfoil toward the trailing edge. As in the low Mach number case, the fluid aft of this point has been swept away into the wake. This is a region of nearly stagnant fluid. No circular fringes are found in the vortex; instead, only half-circular fringes are seen. At $\alpha = 14.5$ deg, the shear layer has reached the trailing edge, and deep stall occurs at $\alpha = 15.5$ deg. The entire sequence lasts only 6–7 deg in angle of attack, which is considerably smaller than the 12-deg range seen for $M = 0.2$. Although the lower Mach number result discussed was obtained at a nondimensional pitch rate that was 50% higher, the range of angle of attack over which dynamic lift is sustained is nearly twice that seen at $M = 0.45$. This confirms the result obtained from the earlier schlieren studies[16] that compressibility promotes stall. These results agree with those reported in Ref. 17 for the oscillating airfoil. However, it should be noted that the two different motion histories will force differences in the details of separation. Dynamic stall of oscillating airfoils is influenced by the constantly changing pitch rate through a cycle and also by hysteresis. These affect all aspects of the flow. The transiently pitching airfoil flow is free of these effects. In addition, since the airfoil continues to pitch to 60 deg, which is well beyond the static stall angle, the development of the post-stall flow and the interactions at the trailing edge can be studied (discussed in Sec. III.A.6), which is of importance to the supermaneuverability problem. This information is also of value in comparing computed results against experiments.

The differences in the vortex size and structure also imply that the overall (global) pressure fields in the incompressible and compressible flow cases are quite different. The sustained presence of a low-pressure region over the airfoil upper surface is evidence that even in the compressible case there is increased lift generated during the dynamic stall process.

5. Leading-Edge-Flow and Stall-Vortex Formation

Carr et al.[17] found that, for an oscillating airfoil, the dynamic stall vortex formed just as the separation bubble burst. It has now been found to be true for the transiently pitching airfoil also. Figure 5 presents some interferograms that demonstrate this result for $M = 0.3$ and $\alpha^+ = 0.03$. At $\alpha = 15$ deg, the fringes enclosing the bubble at a lower angle of attack (not shown) begin to "open up," and vertical fringes (normal to the upper surface) appear near the downstream end of the bubble. This can be seen more clearly at $\alpha = 15.5$ deg. By $\alpha = 15.75$ deg, these fringes extend to about 1.5% of chord above the airfoil and nearly to $0.2c$ along it. The inflection in the fringes very close to the airfoil surface suggests that there is a very slight reverse flow. In contrast, the outer fringes (outside the bubble) proceed only in one direction, toward the trailing edge. The region of reverse flow is less than $0.005c$, and thus it is extremely difficult to detect with experimental techniques other than surface mounted gauges. By $\alpha = 16.5$ deg, the vortex has fully developed and convected to $0.2c$. This rapid succession of events in a very small angle-of-attack range is typical of the evolution of dynamic stall at compressible Mach numbers. However, the interactions between shocks and the boundary layer, along with the events of bubble bursting and vortex formation, are too complicated to be resolved from the images processed so far.

The primary issue that needs to be determined is the origin of the dynamic stall vortex. Whether it originates independently of the separation bubble and simply pushes the back end of the bubble, or the increasing angle of attack makes it no longer possible for the bubble to remain close to the leading edge and moves the reattachment point rearward, allowing the leading-edge vorticity to coalesce, is yet to be found. This is an intriguing issue, especially because the leading-edge flow has already separated, causing the bubble, at a very low angle of attack (much lower than the static stall angle). A plausible description is that the recirculation region in the bubble becomes stronger with increase of angle of attack, eventually forcing a breakdown of the leading-edge flow and leading to the vortex formation. However, a much more careful analysis is needed for clarifying the issues.

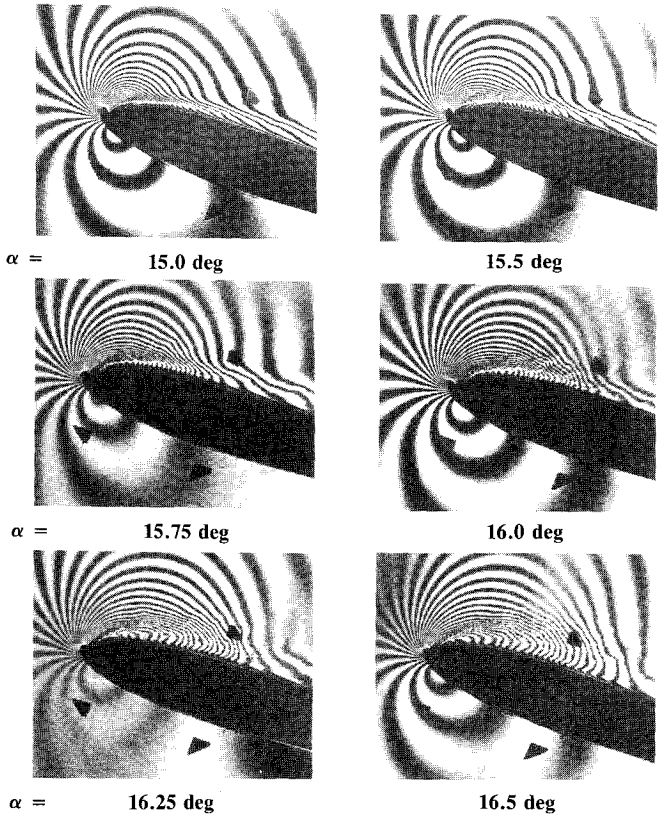

Fig. 5 Details of dynamic stall vortex development over a transiently pitching airfoil; $M = 0.3$ and $\alpha^+ = 0.03$.

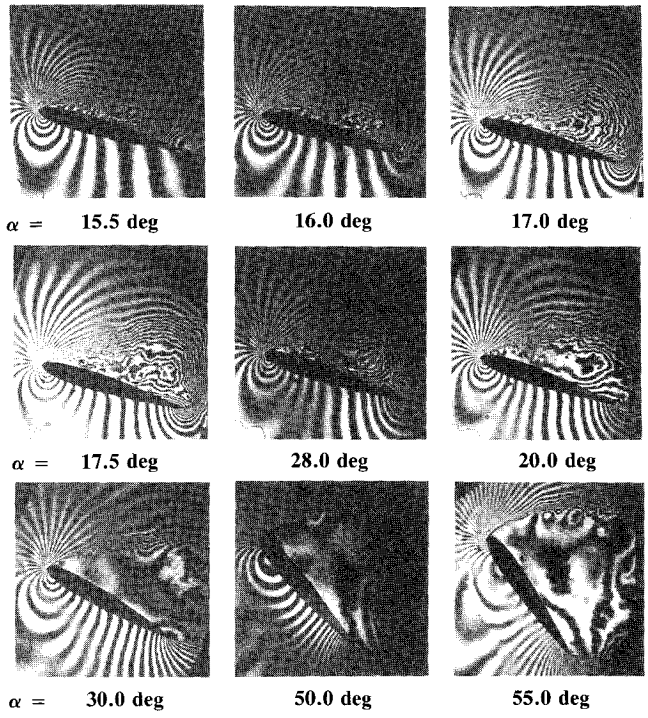

Fig. 6 Trailing-edge flow interactions with dynamic stall vortical flow over a transiently pitching airfoil; $M = 0.45$ and $\alpha^+ = 0.025$.

The formation of a separation bubble indicates that the airfoil leading-edge boundary-layer transition plays a critical role in dynamic stall occurrence. If the boundary layer is modified to transition before the adverse pressure gradient is encountered, it is to be expected that dynamic stall and the associated events occur in a very different manner. This includes stall onset, the details of the vortex formation, and the duration of dynamic lift in the pitching cycle. This is a further aspect that merits a more detailed study.

6. Trailing-Edge Flow Beyond Deep Stall

The flow continues to show interesting features even after deep stall has occurred and the dynamic stall vortex is shed. In Fig. 6, the complete flowfield is shown for just one experimental flow condition ($M = 0.45$ and $\alpha^+ = 0.025$). For this case, the dynamic stall angle of attack (when the dynamic stall vortex leaves the airfoil) is 17 deg; however, the airfoil continues to pitch at a constant rate until $\alpha = 60$ deg. An immediate consequence of vortex shedding under these conditions is an increase in suction pressure at the trailing edge on the lower surface of the airfoil. The trailing-edge suction gradually increases during the dynamic stall process as the airfoil pitches (from $C_p \approx 0.0$ at $\alpha = 0$ deg to $C_p = -0.504$ at $\alpha = 17$ deg). However, at $\alpha = 17.5$ deg, the suction pressure coefficient jumps to -1.04. Also, a counterclockwise vortex begins to form in the near wake at $\alpha = 18$ deg. The birth/growth of this vortex pushes outward the shear layer separating from the leading edge. At $\alpha = 20$ deg, this vortex is shed, and by $\alpha = 30$ deg, only the separated flow can be seen over the upper surface. The same number of fringes (26, corresponding to $C_p = -1.08$), measured from the stagnation point to the lowest velocity point on the upper and lower surface shear layers, seems to indicate that the pressure over the upper surface is nearly constant. However, since the field of view is limited in the facility, the role of the wake and the interaction of the two shear layers cannot be determined to ascertain this fully. As the pitch up continues, shear layer instabilities develop, which roll up into vortices, which appear at $\alpha = 50$ or 55 deg. A large

trailing edge vortex appears from the lower surface at $\alpha = 50$ deg, which rolls up toward the leading-edge shear layer. The peak suction increases slightly with angle of attack, even though the airfoil is in the deep stall state. The stagnation point moves to 0.25 chord point at $\alpha = 55$ deg. Similar features were found for other Mach numbers as well. However, this picture is significantly different from the low Reynolds number and low Mach number results of Walker et al.,[5] who observed two large vortices coexisting on the airfoil suction surface as dynamic stall progressed. This led to a much different airfoil surface pressure distribution than found here. For all of the cases studied here, the trailing-edge vortex was induced as the dynamic stall vortex was shed. At times the leading-edge separated shear layer instabilities produced a large vortex, resulting in a double vortex pattern resembling a vortex street.

B. Quantitative Pressure Field

One of the main advantages of PDI is its truly nonintrusive way of yielding the pressure field. To obtain the average surface pressure distribution by standard techniques in a rapidly changing flow such as the ramping airfoil motion under consideration requires several realizations of the flow, i.e., several pitch-up motions. The PDI technique provides not only the surface pressure map but also the global pressure field instantaneously in one picture, unaffected by history effects. Since a large number of interferograms were obtained at close intervals in angle of attack, a finer set of instantaneous pressure data is in hand now when compared with what can be obtained for an airfoil with a fixed set of pressure taps. The data to be reported are the first global mapping of pressure coefficients that have been obtained for a transiently pitching airfoil under compressibility conditions using PDI.

1. *Effect of Mach Number on Peak Suction Pressure*

Figure 7 shows the peak suction pressure coefficient obtained over the airfoil at different Mach numbers for different pitch rates. The absolute value of C_p in steady flow is lower than in unsteady flows for all Mach numbers tested. Of significance is the relative independence of the peak suction pressure coefficient from the pitch rate for all Mach numbers. It is possible that the formation of the bubble and the strong local compressible conditions have both affected the viscous/inviscid interactions in the flow and thus limited the suction pressure from increasing as the pitch rate is increased. Also, the peak suction decreases dramatically with increasing Mach number. For the lowest Mach number of 0.2, the value of $C_p = -7.1$ corresponds to a local Mach number of 0.58, indicating that compressibility conditions play a role in the process. At $M = 0.45$, the sonic limit is $C_p = -2.78$, and with the suction peak at $C_p = -3.6$, the local flow is supersonic and thus is strongly compressible.

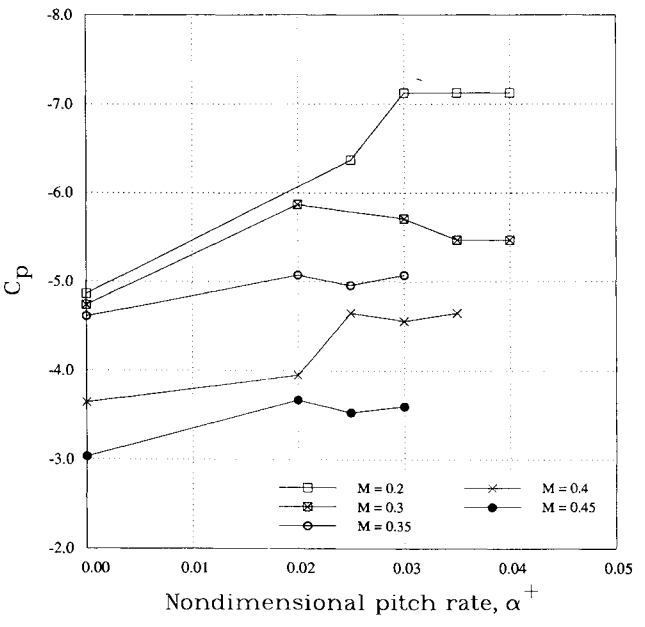

Fig. 7 Transiently pitching airfoil peak suction pressure coefficient at stall vortex formation.

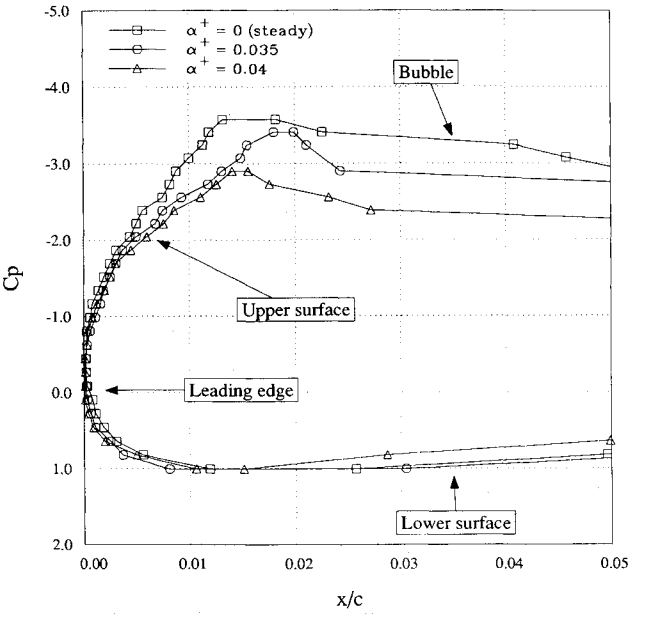

Fig. 8 Effect of pitch rate on pressure development over a transiently pitching airfoil; $M = 0.3$ and $\alpha = 10$ deg.

2. *Effect of Pitch Rate*

In Figure 8, the development of the leading edge-pressure distribution over the first 5% of airfoil chord is compared for $M = 0.3$ for steady flow, $\alpha^+ = 0.035$ and $\alpha^+ = 0.04$ at $\alpha = 10$ deg. It is clear that steady flow develops a stronger suction peak than the unsteady flow cases, with a maximum C_p of -3.6; the suction peak is located at $x/c = 0.012$. The adverse pressure gradient is slower to develop at the higher pitch rates; in fact, the suction level has reached only a value of $C_p = -2.95$ at 10 deg for $\alpha^+ = 0.04$. The pressure distribution for the unsteady cases is less steep than that seen for steady flow. Even though all three cases show a separation bubble, the effect of increasing pitch rate is clearly to delay the flow development over the leading edge, which consequently leads to delay in dynamic stall occurrence.

Figure 9 shows the maximum suction pressure coefficient at different angles of attack for $M = 0.4$. In it, steady flow and unsteady flows at $\alpha^+ = 0.02$ and $\alpha^+ = 0.035$ are compared. The steady flow stalls at $\alpha = 10.8$ deg; at higher angles the leading-edge suction falls rapidly. At $\alpha^+ = 0.02$ the effect of unsteadiness in causing the peak suction pressure coefficient to lag the steady flow values is seen at all angles of attack; the suction levels for $\alpha^+ = 0.035$ lag those of even $\alpha^+ = 0.02$. The rounding of the curves at the top corresponds to the situation when the dynamic stall vortex is in the formative stages. During this stage ($\alpha = 12$–13 deg for $\alpha^+ = 0.02$ and $\alpha = 13$–13.5 deg for $\alpha^+ = 0.035$), the airfoil suction is the maximum. Once the vortex begins to convect, the leading-edge flow slows down, and the suction is steadily lost, even though the angle of attack is still increasing. Despite experimental scatter, it is clear that dynamically pitching airfoils can withstand larger suction peaks than steady airfoils before stall and hence withstand higher flow gradients before dynamic stall occurrence. It is also of value to note that the loss of suction peak in the dynamic case does not mean loss of lift but only the initiation of the dynamic stall vortex.

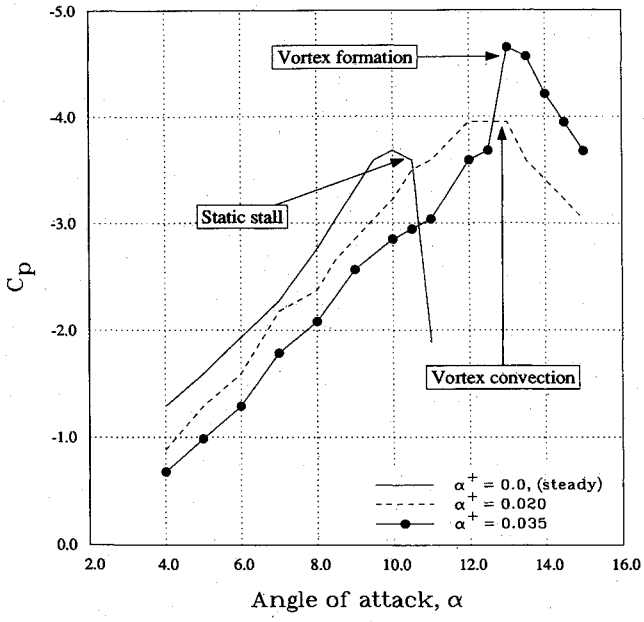

Fig. 9 Effect of pitch rate on peak suction pressure coefficient over a transiently pitching airfoil; $M = 0.4$.

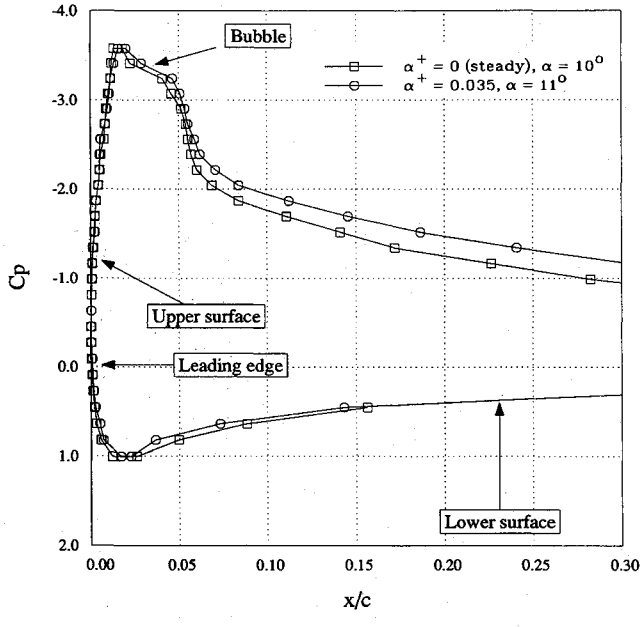

Fig. 10 Comparison of steady and unsteady flows; $M = 0.3$.

Figure 10 shows the pressure distribution at $M = 0.3$ at $\alpha = 10$ deg in steady flow and $\alpha = 11$ deg in unsteady flow at $\alpha^+ = 0.035$. The nearly identical pressure distributions suggest that unsteadiness essentially has introduced a 1-deg lag in the effective angle of attack, including the formation of the separation bubble (see next section), supporting the conclusions drawn from Figs. 8 and 9. As much as 2 deg of decrease in the effective angle of attack for oscillating airfoils was observed by Carr et al.[17] However, as can be expected, the amount of this benefit is determined by the experimental conditions, especially the pitch rate and Mach number.

3. *Airfoil Pressure Distributions*

Airfoil pressure distributions were obtained for different Mach numbers and pitch rates using the method described earlier. A typical case is discussed here for $M = 0.3$ and $\alpha^+ = 0.035$ at different angles of attack in Fig. 11. For this case, Fig. 11a shows that, at $\alpha = 5$ deg, the pressure distribution is smooth, with the suction peak of $C_p = -1.69$ at $x/c = 0.025$. As the airfoil pitches to 7 deg, C_p increases to -2.21. This is accompanied by the upstream movement of the suction peak to $x/c = 0.015$. Along with this, the stagnation point moves from $x/c = 0.01$ to 0.025. As the airfoil pitches to higher angles of attack, further movement of the stagnation point is difficult to detect, until larger angles are reached. At $\alpha = 8$ deg, a separation bubble forms. The pressure plateau following the steep drop in the pressure distribution immediately after the suction peak at $\alpha = 9$ deg confirms this. The bubble extends to $x/c \approx 0.05$. The suction level and the adverse pressure gradient both continue to increase as the airfoil angle of attack is increased. However, Fig. 11b shows that the pressure distributions at $\alpha = 13$ and 14 deg are different from those at $\alpha = 12$ deg only near the suction peak, indicating that the lift and thus the circulation over the airfoil have not changed significantly in this range of pitching. It is also the range when the dynamic stall vortex is initiated as determined by visual analysis of the interferogram images. The suction peak, however, increases with angle of attack and reaches its maximum value of -5.8 when the first imprint of dynamic stall is clearly discernible in the images. At this instant, it appears that the vortex becomes fully organized, and then it begins to convect. The movement of the vortex results in a

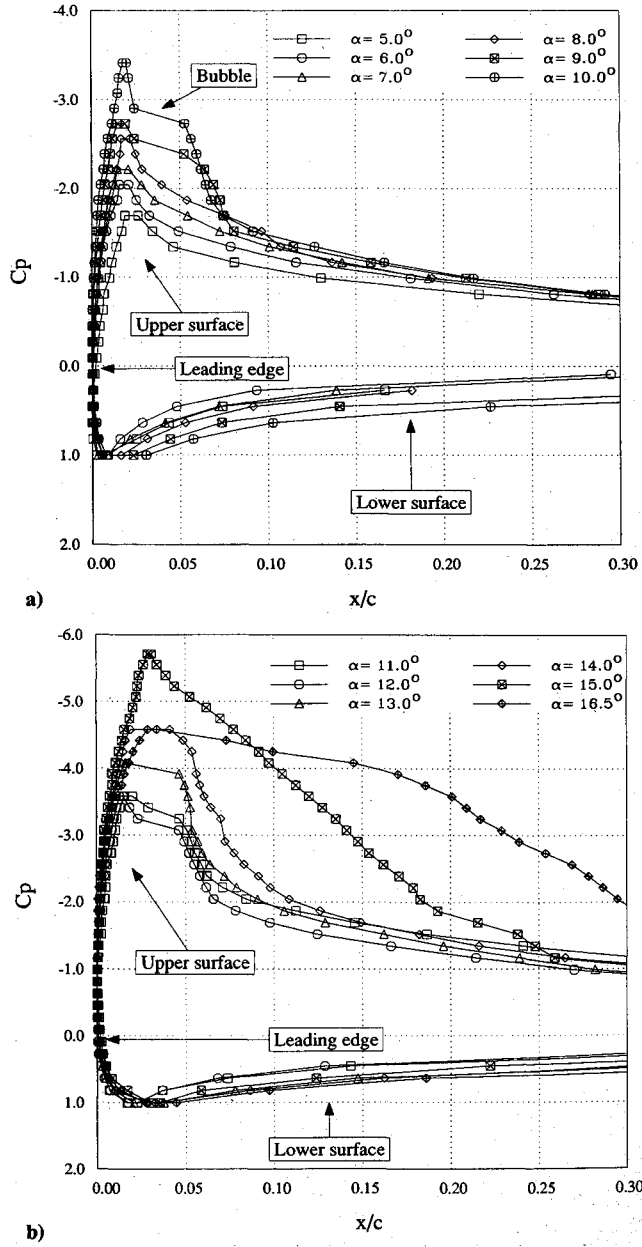

Fig. 11 Pressure distribution over a transiently pitching airfoil; $M = 0.3$ and $\alpha^+ = 0.35$: a) $\alpha = 5$–10 deg, b) $\alpha = 11$–16.5 deg.

slight drop of airfoil suction. However, the pressure distribution changes to the nearly flat-top shape that extends to about $x/c = 0.3$. This increasing region of low pressure over the upper surface is the cause of the vortical lift seen in the flow. Further pitching of the airfoil continues to decrease the suction levels, while spreading the extent of the vortex more over the airfoil, until it is shed past the trailing edge.

IV. Concluding Remarks

A nonintrusive study of the compressibility effects on dynamic stall of a transiently pitching airfoil has been conducted. The study shows the following.

1) Multiple shocks form over the airfoil and are present through the early stages of dynamic stall for a freestream Mach number of 0.4 and higher.

2) Detailed instantaneous pressure distributions show that dynamic stall onset and bursting of the separation bubble occur simultaneously.

3) Flow interferograms and hence the corresponding pressure distributions show that compressibility causes the dynamic stall vorticity to be retained closer to the airfoil surface. The vortical structure in the compressible case is very different than that in the incompressible case.

Acknowledgments

The project was supported by an Air Force Office of Scientific Research Grant MIPR-92-0004 to the Naval Postgraduate School and was monitored by D. B. Fant. Additional support was received from Army Research Office Grant MIPR-130-92, monitored by T. L. Doligalski. The work was carried out in the Fluid Mechanics Laboratory Branch of NASA Ames Research Center. The steady encouragement of S. S. Davis, chief, FML Branch, the support of J. D. Loomis in the conduct of experiments, and the interferogram processing software development effort of P. J. Trosin, Sterling Federal Systems, Inc., are greatly appreciated.

References

[1]Acharya, M., and Metwally, M. H., "Evolution of the Unsteady Pressure Field and Vorticity Production at the Surface of a Pitching Airfoil," AIAA Paper 90-1472, June 1990.

[2]Francis, M. S., and Keese, J. E., "Airfoil Dynamic Stall Performance with Large-Amplitude Motions," *AIAA Journal*, Vol. 23, No. 11, 1985, pp. 1653–1659.

[3]Aihara, Y., Koyama, H., and Murashige, A., "Transient Aerodynamic Characteristics of a Two-Dimensional Airfoil During Stepwise Incidence Variation," *Journal of Aircraft*, Vol. 2, No. 8, 1985, pp. 661–668.

[4]Albertson, J. A., Troutt, T. R., and Kedzie, C. R., "Unsteady Aerodynamic Forces at Low Airfoil Pitching Rates," *Proceedings of the 1st National Fluid Dynamics Conference*, Vol. 1, AIAA, Washington, DC, 1988, pp. 454–462.

[5]Walker, J. M., Helin, H. E., and Strickland, J. H., "An Experimental Investigation of an Airfoil Undergoing Large-Amplitude Pitching Motions," *AIAA Journal*, Vol. 23, No. 8, 1985, pp. 1141, 1142.

[6]Jumper, E. J., Shreck, S. J., and Dimmick, R. L., "Lift-Curve Characteristics for an Airfoil Pitching at Constant Rate," *Journal of Aircraft*, Vol. 24, No. 10, 1987, pp. 680–687.

[7]Lorber, P. F., and Carta, F. O., "Airfoil Dynamic Stall at Constant Pitch Rate and High Reynolds Number," *Journal of Aircraft*, Vol. 25, No. 6, 1988, pp. 548–556.

[8]Visbal, M. R., "Dynamic Stall of a Constant Rate Pitching Airfoil," *Journal of Aircraft*, Vol. 27, No. 5, 1990, pp. 400–407.

[9]Chandrasekhara, M. S., and Carr, L. W., "Flow Visualization Studies of the Mach Number Effects on the Dynamic Stall of an Oscillating Airfoil," *Journal of Aircraft*, Vol. 27, No. 6, 1990, pp. 516–522.

[10]Chandrasekhara, M. S., Carr, L. W., and Ahmed, S., "Comparison of Pitch Rate History on Dynamic Stall," *Proceedings NASA/AFOSR/ARO Workshop on Physics of Forced Unsteady Separation*, NASA-CP-3144, April 1990.

[11]Carr, L. W., and Chandrasekhara, M. S., "Design and Development of a Compressible Dynamic Stall Facility," *Journal of Aircraft*, Vol. 29, No. 3, 1992, pp. 314–318.

[12]Chandrasekhara, M. S., and Carr, L. W., "Design and Development of a Facility for Compressible Dynamic Stall Studies of a Rapidly Pitching Airfoil," *ICIASF'89 RECORD*, IEEE Publication 89CH2762-3, IEEE, New York, 1989, pp. 29–37.

[13]Carr, L. W., Chandrasekhara, M. S., Ahmed, S., and Brock, N. J., "A Study of Dynamic Stall Using Real Time Interferometry," AIAA Paper 91-0007, Jan. 1991.

[14]Brock, N. J., Chandrasekhara, M. S., and Carr, L. W., "A Real Time Interferometry System for Unsteady Flow Measurements," *ICIASF'91 RECORD*, IEEE Publication 91CH3028-8, IEEE, New York, 1991, pp. 423–430.

[15]Goldstein, R. J., "Optical Systems for Flow Measurement: Shadowgraph, Schlieren, and Interferometric Techniques," *Fluid Mechanics Measurements*, Hemisphere, New York, 1985, pp. 377–422.

[16]Chandrasekhara, M. S., Ahmed, S., and Carr, L. W., "Schlieren Studies of Compressibility Effects on Dynamic Stall of Transiently Pitching Airfoils," *Journal of Aircraft*, Vol. 30, No. 2, 1993, pp. 213–220.

[17]Carr, L. W., Chandrasekhara, M. S., and Brock, N. J., "A Quantitative Study of Unsteady Compressible Flow over an Oscillating Airfoil," AIAA Paper 91-1683, June 1991.